Available online at www.sciencedirect.com
SCIENCE DIRECT®
Journal of the European Ceramic Society 25 (2005) 489–499
www.elsevier.com/locate/jeurceramsoc

Oxygen ionic transport in $SrFe_{1-y}Al_yO_{3-\delta}$ and $Sr_{1-x}Ca_xFe_{0.5}Al_{0.5}O_{3-\delta}$ ceramics

A. L. Shaula [a], V. V. Kharton [a,b,*], N. P. Vyshatko [a], E. V. Tsipis [a], M. V. Patrakeev [c], F. M. B. Marques [a], J. R. Frade [a]

[a] *Department of Ceramics and Glass Engineering, CICECO, University of Aveiro, Aveiro 3810-193, Portugal*
[b] *Institute of Physicochemical Problems, Belarus State University, 14 Leningradskaya Str., Minsk 220050, Belarus*
[c] *Institute of Solid State Chemistry, Ural Division of RAS, 91 Pervomayskaya Str., Ekaterinburg 620219, Russia*

Received 14 January 2004; received in revised form 8 March 2004; accepted 13 March 2004
Available online 21 July 2004

Abstract

The oxygen permeability of mixed-conducting $Sr_{1-x}Ca_xFe_{1-y}Al_yO_{3-\delta}$ ($x = 0$–1.0; $y = 0.3$–0.5) ceramics at 850–1000 °C, with an apparent activation energy of 120–206 kJ/mol, is mainly limited by the bulk ionic conduction. When the membrane thickness is 1.0 mm, the oxygen permeation fluxes under pO_2 gradient of 0.21/0.021 atm vary from 3.7×10^{-10} mol s^{-1} cm^{-2} to 1.5×10^{-7} mol s^{-1} cm^{-2} at 950 °C. The maximum solubility of Al^{3+} cations in the perovskite lattice of $SrFe_{1-y}Al_yO_{3-\delta}$ is approximately 40%, whilst the brownmillerite-type solid solution formation range in $Sr_{1-x}Ca_xFe_{0.5}Al_{0.5}O_{3-\delta}$ system corresponds to $x > 0.75$. The oxygen ionic conductivity of $SrFeO_3$-based perovskites decreases moderately on Al doping, but is 100–300 times higher than that of brownmillerites derived from $CaFe_{0.5}Al_{0.5}O_{2.5+\delta}$. Temperature-activated character and relatively low values of hole mobility in $SrFe_{0.7}Al_{0.3}O_{3-\delta}$, estimated from the total conductivity and Seebeck coefficient data, suggest a small-polaron mechanism of p-type electronic conduction under oxidising conditions. Reducing oxygen partial pressure results in increasing ionic conductivity and in the transition from dominant p- to n-type electronic transport, followed by decomposition. The low-pO_2 stability limits of $Sr_{1-x}Ca_xFe_{1-y}Al_yO_{3-\delta}$ seem essentially independent of composition, varying between that of $LaFeO_{3-\delta}$ and the $Fe/Fe_{1-y}O$ boundary. Thermal expansion coefficients of $Sr_{1-x}Ca_xFe_{1-y}Al_yO_{3-\delta}$ ceramics in air are 9×10^{-6} K^{-1} to 16×10^{-6} K^{-1} at 100–650 °C and 12×10^{-6} K^{-1} to 24×10^{-6} K^{-1} at 650–950 °C. Doping of $SrFe_{1-y}Al_yO_{3-\delta}$ with aluminum decreases thermal expansion due to decreasing oxygen nonstoichiometry variations.

Keywords: Perovskites; Membranes; Ionic conductivity; Electrical conductivity; Mixed conductor; (Sr,Ca)(Fe,Al)O_3

1. Introduction

Oxide ceramics with mixed oxygen ionic and electronic conductivity are of great interest for high-temperature electrochemical applications, such as electrodes of solid oxide fuel cells (SOFCs) and dense ceramic membranes for oxygen separation and partial oxidation of light hydrocarbons.[1–4] The use of mixed-conducting membranes enables to decrease the costs of conversion of natural to synthesis gas due to the possibility to integrate oxygen separation, steam reforming and partial oxidation into one single step. Under operation conditions, the ceramic membrane materials should possess oxygen permeation fluxes as high as possible, thermodynamic and dimensional stability in a wide range of oxygen partial pressure and temperature, thermomechanical compatibility with other components of electrochemical devices, and negligible reactivity with gas species such as CO_2, SO_2 and water vapour.

Perovskite-type ferrites $AFeO_{3-\delta}$ (A-rare-earth and/or alkaline-earth metal cation) exhibit a substantial level of the oxygen transport, but have limited stability under large oxygen chemical potential gradients and high thermal expansion.[1,5,6] Moreover, the ferrite phases with high content of alkaline-earth cations may easily interact with carbon dioxide and sulphur oxides. To some extent, these reactions can be suppressed decreasing A-site cation radius, which reduces thermodynamic stability of the reaction products.[7,8] The size of A-site cations also affects transport properties

* Corresponding author. Tel.: +351-234-370263; fax: +351-234-425300.
E-mail address: kharton@cv.ua.pt (V.V. Kharton).

0955-2219/$ – see front matter © 2004 Elsevier Ltd. All rights reserved.
doi:10.1016/j.jeurceramsoc.2004.03.011

of perovskite-related oxides, thus creating an important tool in designing ceramics performance.[9] For example, in the cobaltite system $La_{0.5}Sr_{0.5-x}Ca_xCoO_{3-\delta}$ maximum p-type electronic and oxygen ionic conductivities were observed at $x = 0.2$ and 0.5, respectively.[10] However, for Fe-containing materials based on $AFeO_{3-\delta}$ (A = Sr, Ca), decreasing A-site cation size may promote formation of brownmillerite-like vacancy-ordered phases with a deteriorating influence on the oxygen ionic transport.[11] This makes it necessary to assess phase relationships and ionic conductivity versus Sr:Ca concentration ratio in the perovskite-related systems important for practical applications.

The dimensional stability of $AFeO_{3-\delta}$ ceramics under oxygen chemical potential variations can be improved incorporating isovalent cations with a stable oxidation state, such as Ga^{3+}, into the iron sublattice.[6,12,13] This type of doping suppresses oxygen nonstoichiometry changes and, as a result, decreases thermal and chemically induced expansion of ferrite-based materials. At the same time, Ga doping is associated with a number of specific disadvantages including volatilisation of gallium oxide in reducing atmospheres, possible interaction with catalysts such as Pt or Ni, and high costs.[14] In order to evaluate effects of Al doping as a possible alternative to Ga substitution, the present work was focused on the study of transport properties of $SrFe_{1-y}Al_yO_{3-\delta}$ and $Sr_{1-x}Ca_xFe_{0.5}Al_{0.5}O_{3-\delta}$ ceramics. The data on $SrFeO_{3-\delta}$ and $CaFe_{0.5}Al_{0.5}O_{2.5+\delta}$, used in this work for comparison, were partly published elsewhere.[15–17]

2. Experimental

The powders of $Sr_{1-x}Ca_xFe_{0.5}Al_{0.5}O_{3-\delta}$ ($x = 0$–1.0) and $SrFe_{1-y}Al_yO_{3-\delta}$ ($y = 0.3$–0.5) were prepared via the glycine-nitrate process (GNP), a self-combustion method using glycine as fuel and nitrates of the metal components as oxidant. In the course of synthesis, glycine was added in an aqueous nitrate solution containing metal cations in the stoichiometric proportion (molar glycine/nitrate ratio of 2). The amount of glycine was calculated assuming that N_2, CO_2 and H_2O are the only gaseous products of reaction. The solutions were heated on a hot plate until self-combustion. The resultant powders having a foamed structure were annealed at 800 °C for 2 h to remove residual organic substances, and then ball-milled. Gas-tight ceramics were pressed at 200–250 MPa and sintered at 1200–1375 °C in air for 2–5 h. After sintering and polishing, the samples were annealed in air at 1000 °C for 2–3 h and slowly furnace-cooled to achieve equilibrium with air at low temperatures.

The materials were characterised by X-ray diffraction (XRD), scanning electron microscopy combined with energy dispersive spectroscopy (SEM/EDS), standard picnometric technique, dilatometry, determination of steady-state oxygen permeation fluxes, measurements of the total conductivity (4-probe DC) and Seebeck coefficient as a function of temperature and oxygen partial pressure, and coulometric titration to determine oxygen nonstoichiometry. Experimental techniques and equipment, used for characterisation, were described elsewhere (Refs. 6,11,12,15–19 and references cited). The XRD patterns were collected at room temperature using a Rigaku D/MAX-B diffractometer (Cu Kα, $2\Theta = 20$–80°, step 0.02°, 1 s/step). Structural parameters and the weight ratio of phases in nonsingle-phase materials were refined from the XRD data using the Fullprof program.[20] In all cases, the ceramic samples were gas-tight; the experimental density (Table 1) of single-phase materials was higher than 95% of theoretical density calculated from XRD results. The oxygen ionic conductivity under oxidising conditions was estimated from the data on total conductivity and oxygen permeability, as described elsewhere.[6,17–19] All data on oxygen permeation presented in this work correspond to the membrane feed-side oxygen partial pressure (p_2) fixed at 0.21 atm (atmospheric air).

3. Results and discussion

3.1. Phase relationships and crystal structure

XRD studies of $SrFe_{1-y}Al_yO_{3-\delta}$ ceramics, equilibrated with air, showed formation of a cubic perovskite phase (space group $Pm\bar{3}m$). Whilst $SrFe_{0.7}Al_{0.3}O_{3-\delta}$ was single-phase (Fig. 1), minor impurity peaks were detected in the XRD pattern of $SrFe_{0.5}Al_{0.5}O_{3-\delta}$ ceramics. The phase impurities were identified as $SrAl_2O_4$, Al_2O_3, and

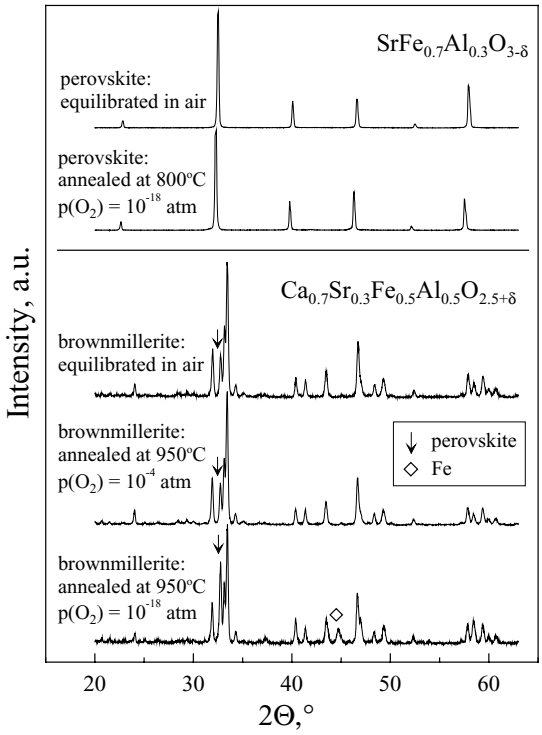

Fig. 1. XRD patterns of $SrFe_{0.7}Al_{0.3}O_{3-\delta}$ and $Ca_{0.7}Sr_{0.3}Fe_{0.5}Al_{0.5}O_{3-\delta}$ ceramics after treatments in various atmospheres.

Table 1
Properties of $Sr_{1-x}Ca_xFe_{1-y}Al_yO_{3-\delta}$ ceramics

Composition	Major phase[a]	Secondary phases[a]	Unit cell parameters (Å)			Density (g cm^{-3})
			a	*b*	*c*	
$SrFe_{0.7}Al_{0.3}O_{3-\delta}$	P	–	3.900(4)	–	–	4.88
$SrFe_{0.5}Al_{0.5}O_{3-\delta}$	P	P′, $SrAl_2O_4$ and Al_2O_3 (<2%)	3.906(9)	–	–	4.65
$Ca_{0.3}Sr_{0.7}Fe_{0.5}Al_{0.5}O_{3-\delta}$	P	$SrAl_2O_4$ (<2%)	3.877(8)	–	–	4.23
$Ca_{0.5}Sr_{0.5}Fe_{0.5}Al_{0.5}O_{3-\delta}$	B	P (38%)	5.614(7)	14.865(4)	5.430(7)	3.86
$Ca_{0.7}Sr_{0.3}Fe_{0.5}Al_{0.5}O_{2.5+\delta}$	B	P (4%)	5.600(9)	14.783(9)	5.403(6)	3.67
$CaFe_{0.5}Al_{0.5}O_{2.5+\delta}$	B	–	5.566(9)	14.514(9)	5.349(1)	3.55
	Thermal expansion coefficients		Apparent activation energies			
	T (°C)	$\bar{\alpha} \times 10^6$ (K^{-1})	Process	*T* (°C)	E_a (kJ/mol)	
$SrFe_{0.7}Al_{0.3}O_{3-\delta}$	100–650	15.4 ± 0.1	Total conductivity	25–535	29.5 ± 0.5	
	650–950	24.0 ± 0.1	Oxygen permeation[b]	850–950	130 ± 15	
$SrFe_{0.5}Al_{0.5}O_{3-\delta}$	100–650	13.5 ± 0.1	Total conductivity	25–515	31.9 ± 0.6	
	650–950	19.1 ± 0.2	Oxygen permeation	750–950	120 ± 6	
$Ca_{0.5}Sr_{0.5}Fe_{0.5}Al_{0.5}O_{3-\delta}$	100–950	12.31 ± 0.02	Total conductivity	190–450	25.3 ± 0.6	
				450–1000	20.6 ± 0.3	
			Oxygen permeation	900–1000	136 ± 9	
$Ca_{0.7}Sr_{0.3}Fe_{0.5}Al_{0.5}O_{2.5+\delta}$	100–950	9.04 ± 0.04	Total conductivity	25–260	27.2 ± 0.4	
				260–975	23.5 ± 0.3	
			Oxygen permeation	950–1000	201	
$CaFe_{0.5}Al_{0.5}O_{2.5+\delta}$	100–600	16.3 ± 0.2	Total conductivity	165–750	56.2 ± 1.2	
				750–975	93.0 ± 6.6	
			Oxygen permeation	850–1000	206 ± 15	

[a] "P" and "B" correspond to perovskite and brownmillerite phases, respectively.
[b] The oxygen permeation activation energies correspond to the pO_2 gradient of 0.21/0.021 atm and the membrane thickness of 1.0 mm.

another cubic perovskite marked as P′ in Table 1; their total amount estimated from the Rietveld refinement results was less than 2 wt.%. Therefore, the maximum solubility of Al^{3+} cations in the iron sublattice of $SrFeO_{3-\delta}$ is close to 40–45%. This estimate is in agreement with the solid solution formation range in the system $La_{0.8}Sr_{0.2}Fe_{1-y}Al_yO_{3-\delta}$, where the perovskite phase exists at $0^\circ \leq y \leq 0.5^\circ$.[21] One should note that the solid solubility of gallium cations in the lattice of strontium ferrite is lower than that of aluminum. For comparison, maximum concentration of Ga^{3+} in $La_{0.3}Sr_{0.7}Fe_{1-y}Ga_yO_{3-\delta}$ perovskites corresponds to $y \approx 0.35$.[6]

The lattice parameters of perovskite-type $Sr(Fe,Al)O_{3-\delta}$ (Table 1) are larger than that of cubic $SrFeO_{3-\delta}$, 3.86 Å (PDF card 34–0638). Moreover, despite the smaller ionic radius of Al^{3+} compared to Fe^{3+} and Fe^{4+},[22] the unit cell volume of $Sr(Fe,Al)O_{3-\delta}$ increases with aluminum concentration. Similar behaviour, earlier observed for $La_{0.3}Sr_{0.7}(Fe,Ga)O_{3-\delta}$,[6] was attributed to a suppressed formation of ordered microdomains due to gallium doping. One alternative hypothesis may refer to decreasing overlap of the electronic orbitals of iron and oxygen ions, resulting from the incorporation of insulating Al^{3+} into the iron sublattice.

The series $Sr_{1-x}Ca_xFe_{0.5}Al_{0.5}O_{3-\delta}$ is characterised by co-existence of two phases, cubic perovskite and brownmillerite (S.G. Ibm2). At $x = 0.3$, the dominant phase is perovskite, with traces of $SrAl_2O_4$ (<2%). For the ceramics with $x = 0.5$ and 0.7, the refined ratio between perovskite and brownmillerite phases was 38:62 and 4:96%, respectively; $CaFe_{0.5}Al_{0.5}O_{2.5}$ was single brownmillerite phase as expected. The concentration range in $Sr_{1-x}Ca_xFe_{0.5}Al_{0.5}O_{3-\delta}$ system, where the solid solution with brownmillerite-type structure exists, can hence be estimated as $0.75 < x \leq 1.00$. The unit cell volume of the brownmillerite phases decreases with decreasing strontium content (Table 1), in agreement with radii of Ca^{2+} and Sr^{2+} cations.[22]

3.2. Thermal expansion

The average thermal expansion coefficients (TECs) of $Sr_{1-x}Ca_xFe_{1-y}Al_yO_{3-\delta}$ ceramics, calculated from dilatometric data in air (Fig. 2), decrease with Al and Ca additions. At temperatures below 650 °C, the TECs vary in the range 9.0×10^{-6} K^{-1} to 15.4×10^{-6} K^{-1} (Table 1). For $SrFe_{1-y}Al_yO_{3-\delta}$, further heating results in increasing thermal expansion coefficients up to 19.1×10^{-6} K^{-1} to 24.0×10^{-6} K^{-1}. This tendency typical for perovskite-like ferrites is associated with oxygen losses on heating.[12,13,18] The average oxidation state of iron cations decreases due to increasing oxygen nonstoichiometry, whilst their size

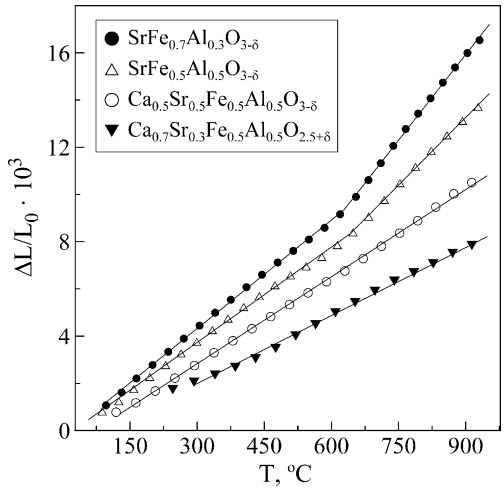

Fig. 2. Dilatometric curves of $Sr_{1-x}Ca_xFe_{1-y}Al_yO_{3-\delta}$ ceramics in air.

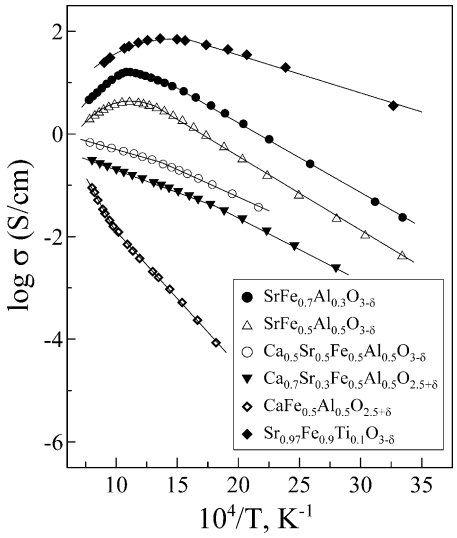

Fig. 3. Temperature dependence of the total conductivity of $Sr_{1-x}Ca_xFe_{1-y}Al_yO_{3-\delta}$ ceramics in air. Data on $Sr_{0.97}Fe_{0.9}Ti_{0.1}O_{3-\delta}$[18] are shown for comparison.

increases; this causes so-called "chemical" contribution to the thermal expansion.[12,13] The incorporation of Al^{3+} having a stable oxidation state suppresses oxygen content variations and, thus, decreases apparent thermal expansion coefficients. Similar trend is characteristic of (La,Sr)(Fe,Ga)$O_{3-\delta}$, the average TECs of which decrease on gallium doping.[12]

On the contrary to $SrFe_{1-y}Al_yO_{3-\delta}$, the dilatometric curves of $Sr_{1-x}Ca_xFe_{0.5}Al_{0.5}O_{3-\delta}$ ($x = 0.5$–0.7) ceramics with high content of brownmillerite phase are almost linear within the studied temperature range (Fig. 2), suggesting that no "brownmillerite → perovskite" transition occurs on heating and the oxygen sublattice remains ordered. Indeed, XRD analysis of samples quenched from 800–950 °C showed no essential changes in the phase composition, in agreement with data on $CaFe_{0.5}Al_{0.5}O_{2.5+\delta}$.[17] Such a behaviour might be advantageous for membrane applications, although further studies are necessary in order to reveal contributions of the constituent phases to total expansion of the ceramic materials.

3.3. Total conductivity

As for thermal expansion, the total conductivity (σ) of $Sr_{1-x}Ca_xFe_{1-y}Al_yO_{3-\delta}$ ceramics decreases when the concentrations of aluminum and calcium increase, Fig. 3. The series $SrFe_{1-y}Al_yO_{3-\delta}$ exhibits a transition to pseudometallic behaviour at temperatures above 800 °C, similar to $SrFeO_{3-\delta}$.[15,16] This trend appears due to decreasing concentration of p-type electronic charge carriers, caused by increasing oxygen nonstoichiometry on heating. The additions of alumina decrease the total concentration of B sites participating in the electronic transport processes and also the concentration of electron holes localised on iron cations, estimated from the Seebeck coefficient data. The role of Ca doping relates mainly to the formation of brownmillerite, where the oxygen content, the concentration of p-type electronic charge carriers and, thus, the total conductivity in air are all lower with respect to perovskite-like ferrites.[17]

The dependencies of total conductivity and Seebeck coefficient (α) on the oxygen partial pressure (Figs. 4 and 5) unambiguously indicate predominant p-type electronic conduction under oxidising conditions. When oxygen pressure is higher than 10^{-5} atm, the values of σ decrease with reducing pO_2, whereas α increases and has positive sign. On

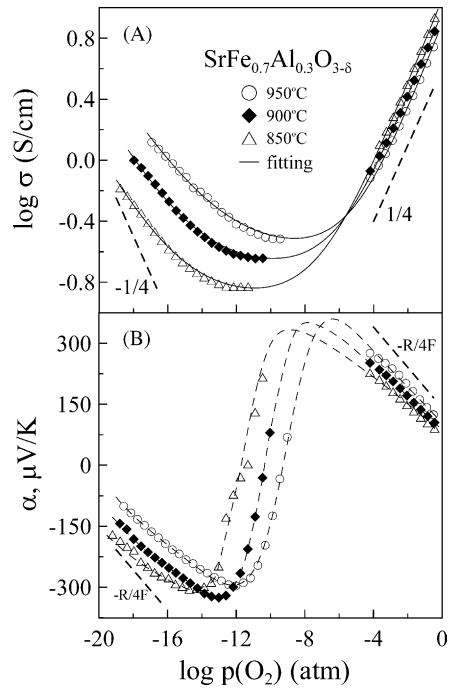

Fig. 4. Oxygen partial pressure dependence of the total conductivity and Seebeck coefficient of $SrFe_{0.7}Al_{0.3}O_{3-\delta}$. Solid lines correspond to the fitting results using Eq. (6) as regression model. Dashed lines are for visual guidance only.

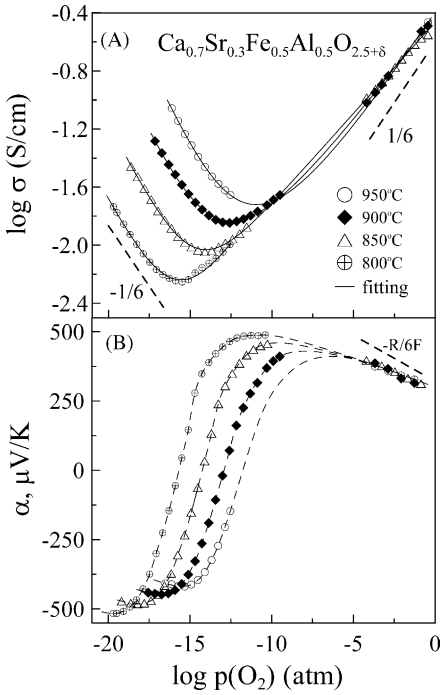

Fig. 5. Oxygen pressure dependence of the total conductivity and Seebeck coefficient of $Ca_{0.7}Sr_{0.3}Fe_{0.5}Al_{0.5}O_{3-\delta}$ ceramics. Solid lines correspond to the fitting results using Eq. (6) as regression model.

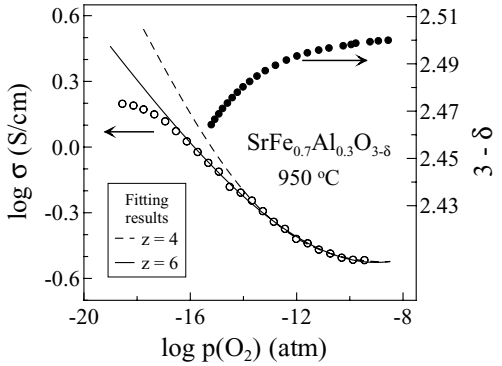

Fig. 6. Oxygen pressure dependence of the total conductivity and oxygen nonstoichiometry of $SrFe_{0.7}Al_{0.3}O_{3-\delta}$ at 950 °C. Dashed and solid lines correspond to the fitting results using Eq. (6) with fixed $z = 4$ and 6, respectively.

further reduction the conductivity reaches minimum and starts to increase due to increasing n-type electronic transport. Respectively, the Seebeck coefficient values become negative, pass through a minimum and then increase. The formation of electron holes can be described as[23]

$$\tfrac{1}{2}O_2 + V_O + 2Fe^{3+} \Leftrightarrow O^{2-} + 2Fe^{4+} \quad (1)$$

with the corresponding equilibrium constant

$$K_{ox} = \frac{[O^{2-}][Fe^{4+}]^2}{[V_O][Fe^{3+}]^2 p(O_2)^{1/2}} = \frac{[O^{2-}]p^2}{[V_O](N-p-n)^2 p(O_2)^{1/2}} \quad (2)$$

where $N = [Fe^{2+}] + [Fe^{3+}] + [Fe^{4+}]$, and $[V_O]$, p and n are the concentrations of oxygen vacancies, p-type (Fe^{4+}) and n-type (Fe^{2+}) electronic charge carriers, respectively. Note that the vacancy concentration, $[V_O]$, is equal to the oxygen nonstoichiometry (δ) multiplied by the volume concentration of perovskite formula units. The charge carrier concentrations are interrelated via the iron disproportionation reaction and the crystal electroneutrality condition:

$$2Fe^{3+} \Leftrightarrow Fe^{2+} + Fe^{4+}$$

$$K_i = \frac{[Fe^{4+}][Fe^{2+}]}{[Fe^{3+}]^2} = \frac{pn}{(N-p-n)^2} \quad (3)$$

$$1 + n = p + 2[V_O] \quad (4)$$

When the oxygen partial pressure is far from the pO_2 range corresponding to conductivity minimum (Fig. 4), one type of electronic charge carriers is expected to dominate, $[Fe^{4+}] \gg [Fe^{2+}]$ namely in oxidising atmospheres and $[Fe^{4+}] \ll [Fe^{2+}]$ under strongly reducing conditions. As the conductivity is proportional to the concentration of charge carriers, their charge and mobility, one can obtain the classical power dependencies for partial p- and n-type electronic conductivities.

$$\sigma_p = \sigma_p^0 p(O_2)^{1/4} \qquad \sigma_n = \sigma_n^0 p(O_2)^{-1/4} \quad (5)$$

where σ_p^0 and σ_n^0 are temperature-dependent constants. The exponent, $\pm 1/4$, corresponds to the situation when the variations of oxygen vacancy concentration are small with respect to total δ values, i.e. the chemical potential of oxygen ions remains essentially constant under a given pO_2 range. If the variations of oxygen ion chemical potential are significant, this theoretical value achieves $\pm 1/6$.[24,25] Fig. 6 illustrates the relationships between oxygen content and total conductivity, by the example of $SrFe_{0.7}Al_{0.3}O_{3-\delta}$ phase at 950 °C.

It should be noted that additional processes, such as defect association and/or local ordering, may affect thermodynamic parameters and defect concentrations in ferrites. In particular, the formation of vacancy-ordered microdomains characteristic of $SrFeO_3$- and $CaFeO_3$-based phases (see, for example, Ref. 11 and references cited) is expected to decrease the concentration of oxygen vacancies participating in the oxygen exchange reactions. This may increase role of minor nonstoichiometry variations in the oxygen-ion chemical potential increment, thus shifting the slope of $\log\sigma$ versus $\log pO_2$ dependencies down to $\pm 1/6$. Therefore, assuming that the ionic conductivity (σ_O) in the pO_2 range around minimum total conductivity is independent of the oxygen pressure, the following simplified model can be used:

$$\sigma = \sigma_O + \sigma_p^0 p(O_2)^{1/m} + \sigma_n^0 p(O_2)^{-1/z} \quad (6)$$

Table 2 lists selected regression parameters of this model; the fitting results are shown in Figs. 4A and 5A by solid lines. In the case of $SrFe_{0.7}Al_{0.3}O_{3-\delta}$, the exponents for p- and n-type electronic conductivities are close to 1/4 and $-1/6$, respectively. To some extent, this asymmetry might

Table 2
Regression parameters of the power dependencies of total conductivity[a] and Seebeck coefficient[b] of $SrFe_{0.7}Al_{0.3}O_{3-\delta}$ on the oxygen partial pressure

T (°C)	Total conductivity			Seebeck coefficient			
	pO_2 (atm)	m	z	pO_2 (atm)	s	pO_2 (atm)	s
950	3×10^{-17}–0.3	3.4 ± 0.1	5.7 ± 0.8	5×10^{-4}–0.3	4.3 ± 0.2	3×10^{-19}–8×10^{-15}	5.7 ± 0.2
900	1×10^{-18}–0.3	3.5 ± 0.1	5.1 ± 0.6	6×10^{-5}–0.3	4.9 ± 0.2	6×10^{-20}–1×10^{-14}	5.7 ± 0.3
850	2×10^{-19}–0.3	3.6 ± 0.1	4.9 ± 0.8	6×10^{-5}–0.3	5.3 ± 0.2	6×10^{-20}–3×10^{-16}	5.8 ± 0.6

[a] Model for total conductivity vs. oxygen pressure (atm): $\sigma = \sigma_p^0 p(O_2)^{1/m} + \sigma_O + \sigma_n^0 p(O_2)^{-1/z}$.
[b] Model for Seebeck coefficient vs. oxygen pressure (atm): $\alpha = -(R/F)(1/s)\ln p(O_2) + A$.

be related to the fact that the oxygen pressure range studied in this work was limited by the atmospheric pressure and phase stability boundary at high and low pO_2, correspondingly. In addition, the range of moderately reducing pO_2 was excluded from the consideration due to errors associated with stagnated diffusion processes in the gas phase.[26] As a result, the studied pO_2 interval was substantially asymmetric with respect to the conductivity minima (Fig. 4). At the same time, the slopes of linear parts of the dependencies α versus $\ln pO_2$ are close to $-R/4F$ and $-R/6F$ in oxidising and reducing conditions, respectively (Table 2). For an ideal mixed conductor where $p \sim {pO_2}^{1/4}$ and $n \sim {pO_2}^{-1/4}$, these values should be equal to $-R/4F$.[24,27] This suggests that $n \sim {pO_2}^{-1/6}$ under reducing conditions. In other words, the concentration of n-type electronic charge carriers seems affected by defect association and/or partial oxygen-vacancy ordering, decreasing the concentration of free vacancies participating in the oxygen exchange process at low pO_2.[11,18] The data shown in Fig. 4 and Table 2 correspond well to a transition from disordered perovskite to partially ordered material, where the moderate nonstoichiometry variations have a significant effect on the oxygen ion chemical potential as most oxygen vacancies are trapped.

3.4. Seebeck coefficient

The fitting results using Eq. (6) and the oxygen permeation data discussed below show that the total conductivity of $SrFe_{0.7}Al_{0.3}O_{3-\delta}$ under oxidising conditions is predominantly p-type electronic, with ionic contribution lower than 1%. In this situation, the Seebeck coefficient for a hopping conduction mechanism can be expressed as:[24,27]

$$\alpha = \frac{R}{F}\left[\ln\left(\frac{N-p}{\beta p}\right) + \frac{q}{RT}\right] \quad (7)$$

where β is a factor due to spin and orbital degeneracy, N is the concentration of sites participating in the hole transport and q is the transported heat of holes. For $SrFe_{0.7}Al_{0.3}O_{3-\delta}$ the value of N is equal to the total concentration of Fe cations, β is equal to 6/5, and q can be neglected (Ref. 15 and references cited). Taking the electroneutrality condition into account, one can calculate the hole concentration and oxygen nonstoichiometry from the Seebeck coefficient data. Then, assuming $\sigma_p \approx \sigma$ under oxidising atmospheres, the values of hole concentration and total conductivity may be used to estimate hole mobility:

$$\sigma_p = ep\mu_p \quad (8)$$

The results of such estimations are shown in Figs. 7 and 8. When the hole concentration is fixed, the hole mobility in $SrFe_{0.7}Al_{0.3}O_{3-\delta}$ follows Arrhenius-type dependence on temperature, indicative of a small-polaron conductivity mechanism. Also, the absolute values of hole mobility, 0.009–0.016 $cm^2\,V^{-1}\,s^{-1}$ at 800–950 °C, are essentially lower than 0.1 $cm^2\,V^{-1}\,s^{-1}$, which can be considered as a characteristic criterion between the polaron and broad-band conductors. On the other hand, the mobility activation energy was found to progressively decrease with increasing pO_2 when the oxygen-ion and hole concentrations increase (inset in Fig. 7). This tendency is associated with increasing oxidation state of Fe cations and lattice contraction, leading to a greater overlap of iron and oxygen electron orbitals and, thus, to a stronger covalence of the Fe–O–Fe bonds and higher delocalisation of the electron charge carriers. As a particular result, the adequacy of Eqs. (4) and (7) for the description of nonstoichiometry-thermopower

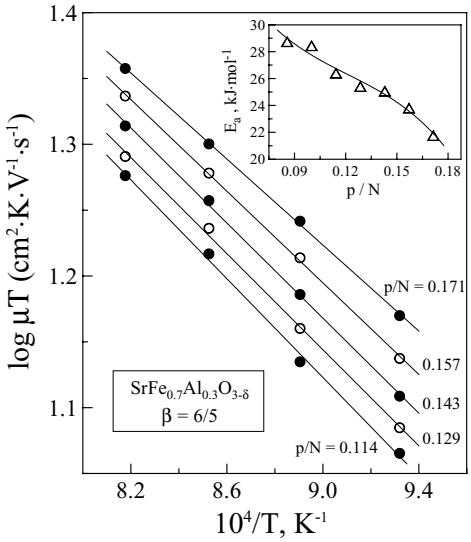

Fig. 7. Temperature dependence of hole mobility in $SrFe_{0.7}Al_{0.3}O_{3-\delta}$, estimated from the total conductivity and Seebeck coefficient data, at fixed hole concentration. Inset shows mobility activation energy vs. relative concentration of electron holes.

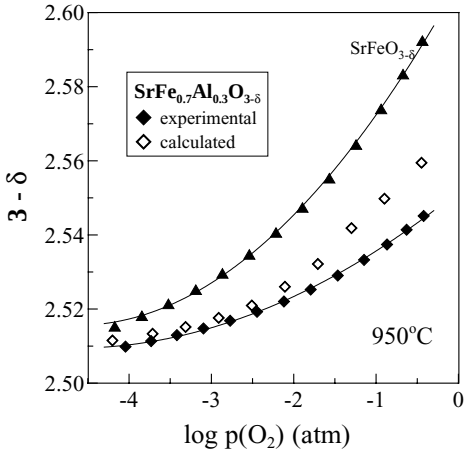

Fig. 8. Comparison of the experimental and calculated values of oxygen content in $SrFe_{0.7}Al_{0.3}O_{3-\delta}$ at 950 °C. The estimates of oxygen nonstoichiometry are obtained from the Seebeck coefficient data using Eqs. (4) and (7). Closed triangles show experimental data on the nonstoichiometry of $SrFeO_{3-\delta}$.

relationship becomes worse (Fig. 8). At oxygen pressures of 10^{-4}–10^{-2} atm, the oxygen deficiency of $SrFe_{0.7}Al_{0.3}O_{3-\delta}$ estimated from the Seebeck coefficient is very close to experimental data measured by the coulometric titration technique. However, progressive hole delocalisation at $pO_2 > 10^{-2}$ atm causes increasing difference between the experimental and calculated δ values. Another necessary comment is that, similar to $La_{0.3}Sr_{0.7}(Fe,Ga)O_{3-\delta}$ solid solutions,[12] oxygen nonstoichiometry of $SrFe_{0.7}Al_{0.3}O_{3-\delta}$ perovskite is significantly higher compared to undoped $SrFeO_{3-\delta}$.

3.5. Phase stability

At oxygen partial pressure lower than 10^{-17}–10^{-20} atm, the conductivity starts to deviate from the power dependence Eq. (6) shown in Fig. 9 by solid lines; further reduction leads to irreversible degradation of the electrical properties. The oxygen pressure, at which the slope of $\log\sigma$ versus $\log pO_2$ curves starts to change, was considered as the stability limit at a given temperature. Fig. 10 presents the stability boundary of $SrFe_{0.7}Al_{0.3}O_{3-\delta}$ and $Ca_{0.7}Sr_{0.3}Fe_{0.5}Al_{0.5}O_{3-\delta}$ at reduced oxygen partial pressures as estimated from the data on the total conductivity. It should be mentioned that, although the tendency to form brownmillerite-like phases with ordered oxygen sublattice should increase on reduction when the oxygen nonstoichiometry increases, no essential phase changes detectable by XRD were observed in the ceramic samples annealed at 800–950 °C in atmospheres with various pO_2. As an example, Fig. 1 presents XRD pattern of $SrFe_{0.7}Al_{0.3}O_{3-\delta}$ annealed in flowing 10% H_2–90% N_2 mixture with $pO_2 \approx 10^{-18}$ atm at 800 °C for 10 h; apparently the ceramics remains single perovskite phase. Most likely, such a behaviour appears due to kinetic reasons preventing the transition

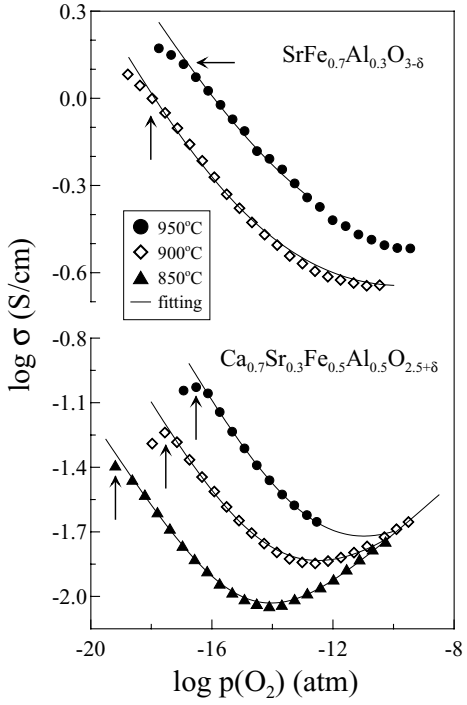

Fig. 9. Oxygen partial pressure dependence of the total conductivity of $SrFe_{0.7}Al_{0.3}O_{3-\delta}$ and $Ca_{0.7}Sr_{0.3}Fe_{0.5}Al_{0.5}O_{3-\delta}$ ceramics in reducing atmospheres. Arrows show data points corresponding to the approximate stability boundary. Solid lines correspond to the fitting results using Eq. (6) as regression model.

from partially ordered perovskite into brownmillerite. In the brownmillerite lattice, the occupation of two nonequivalent B sites by the Fe and Al cations is not random.[17] The "perovskite → brownmillerite" transition may hence require cation diffusion, which is stagnated in dense ceramic materials at 800–900 °C. Despite stabilisation mechanism, the XRD results show that the phase composition of $Sr_{1-x}Ca_xFe_{1-y}Al_yO_{3-\delta}$ ceramics sintered in air (Table 1) is kept until the segregation of metallic Fe in reducing

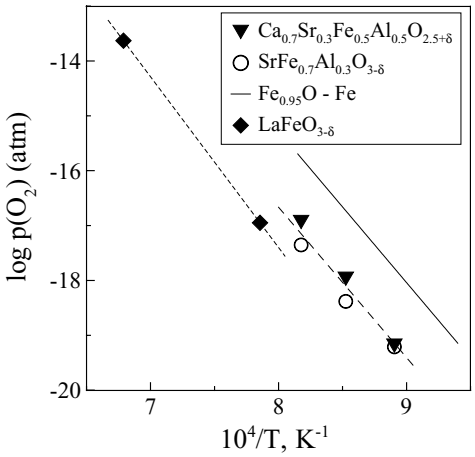

Fig. 10. Stability limits of $SrFe_{0.7}Al_{0.3}O_{3-\delta}$ and $Ca_{0.7}Sr_{0.3}Fe_{0.5}Al_{0.5}O_{3-\delta}$ as estimated from the data on total conductivity. Literature data on $Fe_{1-\delta}O$[30] and $LaFeO_{3-\delta}$[28,29] are shown for comparison.

atmospheres occurs (Fig. 1). The low-pO_2 stability boundaries of $SrFe_{0.7}Al_{0.3}O_{3-\delta}$ and $Ca_{0.7}Sr_{0.3}Fe_{0.5}Al_{0.5}O_{3-\delta}$ are very similar, being slightly higher than that of $LaFeO_{3-\delta}$.[28,29] If compared to $Fe/Fe_{1-\gamma}O$ boundary,[30] the reduction of all perovskite-related phases occurs at lower pO_2 values, as expected from thermodynamics. The standard enthalpy, which can be estimated from the slope of linear van't Hoff dependence, $\log pO_2$ versus $1/T$, is similar for all Fe-containing oxides (Fig. 10).

3.6. Oxygen permeation versus membrane thickness

Selected examples, illustrating typical relationships between oxygen permeation fluxes (j) through dense $Sr_{1-x}Ca_xFe_{1-y}Al_yO_{3-\delta}$ ceramics and membrane thickness (d), are presented in Figs. 11 and 12. The specific oxygen permeability, $J(O_2)$, was calculated as[6,9,11,18]

$$j = \frac{J(O_2)}{d} \ln\left(\frac{p_2}{p_1}\right) \quad (9)$$

where p_1 and p_2 are the oxygen partial pressures at the membrane permeate and feed sides, respectively. As $J(O_2)$ is proportional to $j \times d$ by definition, the specific permeability should be thickness-independent if the overall oxygen transport is predominantly limited by the bulk ionic conduction. This situation indeed takes place, within the limits of experimental uncertainty. Although the data in Figs. 11 and 12 might be indicative of a minor surface effect, which is reflected by a slight increase in the $J(O_2)$ values with increasing d[6,11,18] and becomes more pronounced on reducing temperature and oxygen partial pressure, the observed variations of $J(O_2)$ values are comparable to the experimental error. As a result, the difference in ionic conductivity values, estimated from the oxygen permeation data for the membranes with different thickness, are statistically insignificant; one example is shown in Fig. 13. Note that negligible surface exchange limitations to oxygen transport are observed for numerous ferrite phases with moderate level of the ionic conductivity.[19]

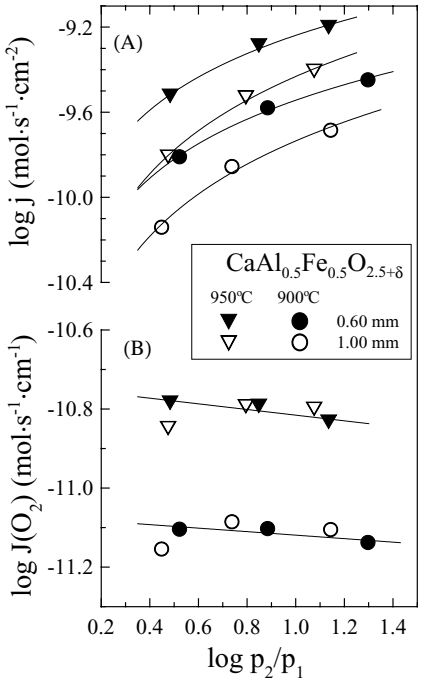

Fig. 11. Oxygen permeation fluxes (A) and specific oxygen permeability (B) of $CaFe_{0.5}Al_{0.5}O_{2.5+\delta}$ brownmillerite ceramics as function of the oxygen partial pressure gradient.

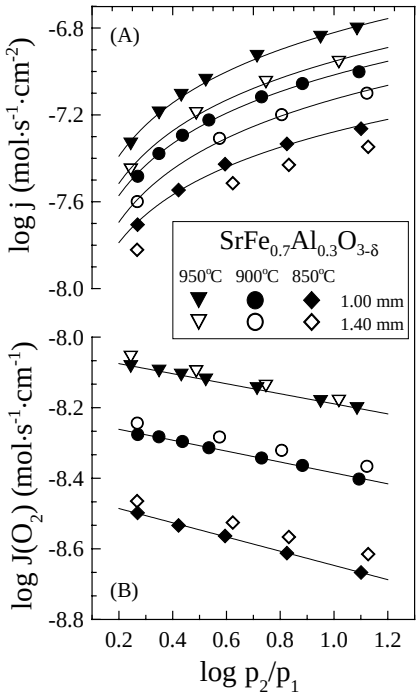

Fig. 12. Oxygen permeation fluxes (A) and specific oxygen permeability (B) of $SrFe_{0.7}Al_{0.3}O_{3-\delta}$ perovskite ceramics as function of the oxygen partial pressure gradient.

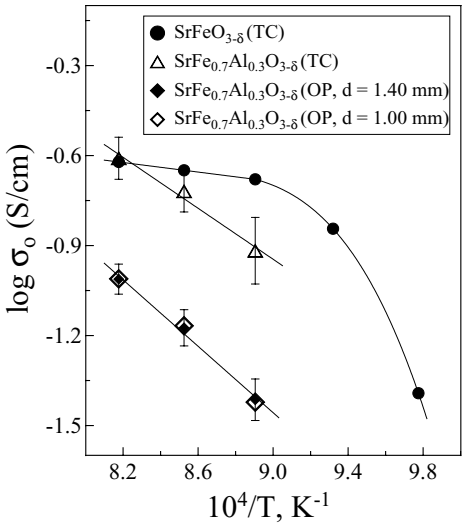

Fig. 13. Comparison of the oxygen ionic conductivity of $SrFeO_{3-\delta}$ and $SrFe_{0.7}Al_{0.3}O_{3-\delta}$, determined from the data on oxygen permeation (OP), and calculated from the pO_2 dependencies of total conductivity (TC) by Eq. (6) as illustrated by Fig. 4.

3.7. Ionic transport

Fig. 13 compares the ionic conductivity of $SrFe_{0.7}Al_{0.3}O_{3-\delta}$ in oxidising and reducing conditions, evaluated from the oxygen permeation data and calculated from the pO_2 dependencies of total conductivity (TC) using Eq. (6) as regression model, respectively. As for $La_{0.3}Sr_{0.7}FeO_{3-\delta}$,[6] $SrFe_{0.7}Al_{0.3}O_{3-\delta}$ exhibits a higher ionic conduction in reducing atmospheres, whilst the activation energy is essentially independent of the oxygen pressure. In agreement with random walk theory for ionic transport,[31] this behaviour results from increasing oxygen vacancy concentration in the perovskite lattice, with the ion migration enthalpy independent of oxygen chemical potential. One should mention that such trend does not contradict to the model Eq. (6) since at oxygen pressures lower than 10^{-4} atm, when the ionic contribution to the total conductivity becomes significant, the oxygen deficiency tends to a plateau characteristic for p–n transitions in mixed conductors (Fig. 8). At the same time, the variations of oxygen nonstoichiometry (5–10%) are considerably lower than the changes in ionic conductivity on reducing pO_2, 40–50% (Fig. 13). This suggests that a significant part of oxygen vacancies in $SrFe_{0.7}Al_{0.3}O_{3-\delta}$ is blocked, presumably in the ordered microdomains.[11,18] In case of undoped $SrFeO_{3-\delta}$, the temperature dependence of ionic conductivity in reducing atmospheres is nonlinear due to a transition from vacancy-ordered brownmillerite into perovskite modification on heating.[16] No such transition is observed for $SrFe_{0.7}Al_{0.3}O_{3-\delta}$ at temperatures above 800 °C, and the ionic conductivity of the latter follows an Arrhenius trend.

Figs. 14 and 15 presents a comparison of the oxygen permeation fluxes through $Sr_{1-x}Ca_xFe_{1-y}Al_yO_{3-\delta}$ membranes. For the materials where the level of ionic conduction is determined by disordered perovskite phases, the apparent activation energies (E_a) vary in the narrow range 120–136 kJ/mol (Table 1). In the case of brownmillerite phases where the oxygen sublattice is ordered, completely or partially, the E_a values are higher than 200 kJ/mol. Respectively, the level of oxygen permeation and ionic conduction in Sr(Fe,Al)O_3-based ceramics is 10^2–10^3 times higher than those in materials derived from $CaFe_{0.5}Al_{0.5}O_{2.5+\delta}$. The structural aspects, which may be responsible for such behaviour, were analysed elsewhere.[16,17]

Thus, although the substitution of Sr with Ca suppresses thermal expansion and may be useful to increase stability in CO_2- and SO_x-containing atmospheres, this type of doping leads to a drastic decrease in ionic transport. The brownmillerite-type mixed conductors, where the A sublattice is occupied by calcium, are hence inappropriate for the use in thick ceramic membranes due to relatively low oxygen permeation. However, these materials may be advantageous for the applications in thin-film membranes, where the performance is not limited by the ionic conduction and the low thermal expansion is extremely important to provide sufficient stability with respect to thermal cycling. For the use in thick tubular membranes, the maximum performance is expected for $SrFe_{1-y}Al_yO_{3-\delta}$ ($y = 0.30$–0.40) heavily doped with aluminum in order to decrease thermal and chemically induced expansion down to possible minimum. The oxygen permeability of $SrFe_{1-y}Al_yO_{3-\delta}$ ceramics is higher than that of $Sr_{0.97}Fe_{0.9}Ti_{0.1}O_{3-\delta}$, another potentially interesting membrane composition.[18] Studies of the catalytic and thermochemical properties of $SrFe_{1-y}Al_yO_{3-\delta}$ are now in progress.

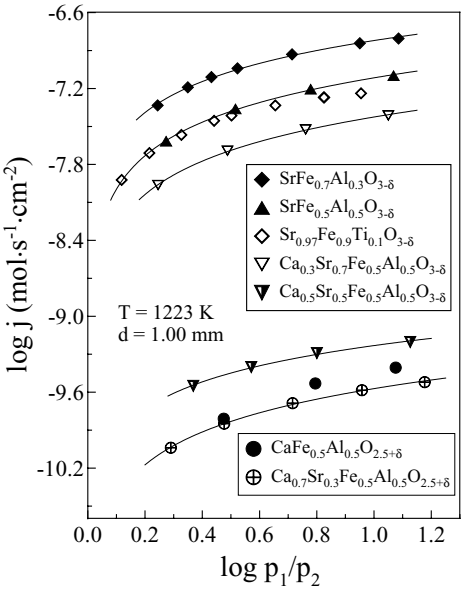

Fig. 14. Comparison of the oxygen permeation fluxes $Sr_{1-x}Ca_xFe_{1-y}Al_yO_{3-\delta}$ membranes with fixed thickness at 950 °C. Solid lines are for visual guidance only.

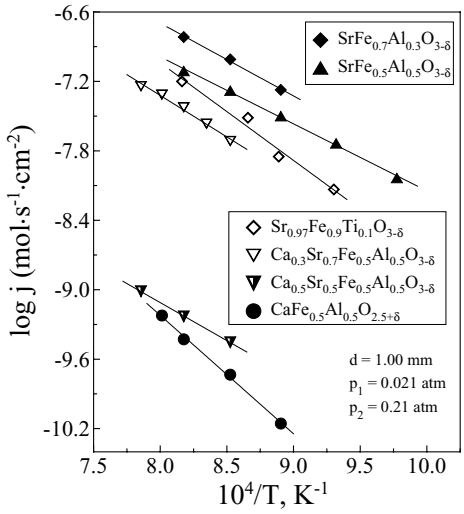

Fig. 15. Temperature dependence of the oxygen permeation fluxes through $Sr_{1-x}Ca_xFe_{1-y}Al_yO_{3-\delta}$ membranes under fixed oxygen partial pressure gradient. Data on $Sr_{0.97}Fe_{0.9}Ti_{0.1}O_{3-\delta}$[18] are shown for comparison.

4. Conclusions

Dense $Sr_{1-x}Ca_xFe_{1-y}Al_yO_{3-\delta}$ ($x = 0$–1.0; $y = 0.3$–0.5) ceramics were prepared via glycine-nitrate process and characterised by XRD, SEM/EDS, dilatometry, measurements of total conductivity and Seebeck coefficient, and determination of steady oxygen permeation fluxes. In the systems $SrFe_{1-y}Al_yO_{3-\delta}$ and $Sr_{1-x}Ca_xFe_{0.5}Al_{0.5}O_{3-\delta}$, the solid solutions with perovskite- and brownmillerite-type structures are formed at approximately $y = 0$–0.40 and $x = 0.75$–1.0, respectively. The average thermal expansion coefficients calculated from dilatometric data are $9 \times 10^{-6}\,K^{-1}$ to $16 \times 10^{-6}\,K^{-1}$ at 100–650 °C and $12 \times 10^{-6}\,K^{-1}$ to $24 \times 10^{-6}\,K^{-1}$ at 650–950 °C in air. The oxygen permeation through $Sr_{1-x}Ca_xFe_{1-y}Al_yO_{3-\delta}$ membranes at 850–1000 °C is mainly determined by the bulk ionic conduction. The partial ionic and p-type electronic conductivities both decrease with increasing Al and Ca concentrations. Reducing pO_2 results in a transition from the dominant p-type electronic transport, which occurs via a small-polaron mechanism, to n-type conduction, whilst the ionic conductivity increases.

Acknowledgements

This work was supported by the FCT, Portugal (POCTI program and project BD/6595/2001), the NATO Science for Peace program (project 978002), and the INTAS (project 00276).

References

1. Bouwmeester, H. J. M. and Burggraaf, A. J., Dense ceramic membranes for oxygen separation. In *Fundamentals of Inorganic Membrane Science and Technology*, ed. A. J. Burggraaf and L. Cot. Elsevier, Amsterdam, 1996, pp. 435–528.
2. Mazanec, T. J., Electropox gas reforming. In *Ceramic Membranes I, Vol PV 95-24*, ed. H. U. Anderson, A. C. Khandkar and M. Liu. The Electrochemical Society, Pennigton, NJ, 1997, pp. 16–28.
3. Dyer, P. N., Richards, R. E., Russek, S. L. and Taylor, D. M., Ion transport membrane technology for oxygen separation and syngas production. *Solid State Ionics* 2000, **134**, 21–33.
4. Kilner, J., Benson, S., Lane, J. and Waller, D., Ceramic ion conducting membranes for oxygen separation. *Chem. Ind.* 1997, **17**, 907–911.
5. Pei, S., Kleefisch, M. S., Kobylinski, T. P., Faber, J., Udovich, C. A., Zhang-McCoy, V. *et al.*, Failure mechanisms of ceramic membrane reactors in partial oxidation of methane to synthesis gas. *Catal. Lett.* 1995, **30**, 201–212.
6. Kharton, V. V., Yaremchenko, A. A., Viskup, A. P., Patrakeev, M. V., Leonidov, I. A., Kozhevnikov, V. L. *et al.*, Oxygen permeability and ionic conductivity of perovskite-related $La_{0.3}Sr_{0.7}Fe(Ga)O_{3-\delta}$. *J. Electrochem. Soc.* 2002, **149**, E125–E135.
7. Kreuer, K. D., Strategies in the development of proton conducting oxides for fuel cell applications. In *Ionic and Mixed Conducting Ceramics III, Vol PV 97-24*, ed. T. A. Ramanarayanan. The Electrochemical Society, Pennington, NJ, 1998, pp. 17–27.
8. Yokokawa, H., Sakai, N., Kawada, T. and Dokiya, M., Thermodynamic stabilities of perovskite oxides for electrodes and other electrochemical materials. *Solid State Ionics* 1992, **52**, 43–56.
9. Kharton, V. V., Yaremchenko, A. A. and Naumovich, E. N., Research on the electrochemistry of oxygen ion conductors in the former Soviet Union. II. Perovskite-related oxides. *J. Solid State Electrochem.* 1999, **3**, 303–326.
10. Kononov, R. P., Demin, A. K. and Esina, N. O., Oxygen permeation through $La_{0.5}Sr_{0.5-x}Ca_xCoO_{3-\delta}$ ($x = 0$–0.5) membranes. In *Proc. 10th IUPAC Conf. on High Temperature Materials Chemistry, Part II*, ed. K. Hilpert, F. W. Froben and L. Singheiser. Forschungszentrum Julich, Germany, 2000, pp. 703–705.
11. Kharton, V. V., Figueiredo, F. M., Kovalevsky, A. V., Viskup, A. P., Naumovich, E. N., Jurado, J. R. *et al.*, Oxygen diffusion in, and thermal expansion of, $SrTiO_{3-\delta}$- and $CaTiO_{3-\delta}$-based materials. *Defect Diffus. Forum* 2000, **186–187**, 119–136.
12. Kharton, V. V., Yaremchenko, A. A., Patrakeev, M. V., Naumovich, E. N. and Marques, F. M. B., Thermal and chemical induced expansion of $La_{0.3}Sr_{0.7}(Fe,Ga)O_{3-\delta}$ ceramics. *J. Eur. Ceram. Soc.* 2003, **23**, 1417–1426.
13. Schwartz, M., White, J. H. and Sammells, A. F., *Solid state oxygen anion and electron mediating membrane and catalytic membrane reactors containing them*. US Patent 6214757, 10 April, 2001.
14. Yamaji, K., Horita, T., Ishikawa, M., Sakai, N. and Yokokawa, H., Chemical stability of the $La_{0.9}Sr_{0.1}Ga_{0.8}Mg_{0.2}O_{2.85}$ electrolyte in a reducing atmosphere. *Solid State Ionics* 1999, **121**, 217–224.
15. Patrakeev, M. V., Shilova, J. A., Mitberg, E. B., Lakhtin, A. A., Leonidov, I. A. and Kozhevnikov, V. L., Oxygen intercalation in strontium ferrite: evolution of thermodynamics and electron transport properties. In *New Trends in Intercalation Compounds for Energy Storage*, ed. C. Julien, J. P. Pereira-Ramos and A. Momchilov. Kluwer, Dordrecht, Netherlands, 2002, pp. 565–572.
16. Kozhevnikov, V. L., Leonidov, I. A., Patrakeev, M. V., Mitberg, E. B. and Poeppelmeier, K. R., Electrical properties of the ferrite $SrFeO_y$ at high temperatures. *J. Solid State Chem.* 2000, **158**, 320–326.
17. Kharton, V. V., Marozau, I. P., Vyshatko, N. P., Shaula, A. L., Viskup, A. P., Naumovich, E. N. *et al.*, Oxygen ionic conduction in brownmillerite $CaAl_{0.5}Fe_{0.5}O_{2.5+\delta}$. *Mater. Res. Bull.* 2003, **38**, 773–782.
18. Kharton, V. V., Kovalevsky, A. V., Tsipis, E. V., Viskup, A. P., Naumovich, E. N., Jurado, J. R. *et al.*, Mixed conductivity and stability of A-site-deficient $Sr(Fe,Ti)O_{3-\delta}$ perovskites. *J. Solid State Chem.* 2002, **7**, 30–36.
19. Kharton, V. V., Shaula, A. L., Naumovich, E. N., Vyshatko, N. P., Marozau, I. P., Viskup, A. P. *et al.*, Ionic transport in $Gd_3Fe_5O_{12}$- and $Gd_3Fe_5O_{12}$-based garnets. *J. Electrochem. Soc.* 2003, **150**, J33–J42.
20. Rodriguez-Carvajal, J., Recent advances in magnetic-structure determination by neutron powder diffraction. *Phys. B* 1993, **192**, 55–69.
21. Holc, J., Kuščer, D., Hrovat, M., Bernik, S. and Kolar, D., Electrical and microsructural characterisation of $La_{0.8}Sr_{0.2}Fe_{1-x}Al_xO_3$ and $La_{0.8}Sr_{0.2}Mn_{1-x}Al_xO_3$ as possible SOFC cathode materials. *Solid State Ionics* 1997, **95**, 259–268.
22. Shannon, R. D., Revised effective ionic-radii and systematic studies of interatomic distances in halides and chalcogenides. *Acta Cryst.* 1976, **A32**, 751–767.
23. Mizusaki, J., Yoshihiro, M., Yamauchi, S. and Fueki, K., Nonstoichiometry and defect structure of the perovskite-type oxides $La_{1-x}Sr_xFeO_{3-\delta}$. *J. Solid State Chem.* 1985, **58**, 257–266.
24. Kofstad, P., *Nonstoichiometry, Diffusion and Electrical Conductivity in Binary Metal Oxides*. Wiley-Interscience, NY, 1972.
25. Rotman, S. R. and Tuller, H. L., Defect-property correlations in garnet crystals. III. The electrical conductivity and defect structure of luminescent nickel-doped yttrium aluminum garnet. *J. Appl. Phys.* 1987, **62**, 1305–1312.
26. Marques, F. M. B. and Wirtz, G. P., Oxygen fugacity control in nonflowing atmospheres. I. Experimental observations in CO/CO_2 and O_2/N_2 mixtures. *J. Am. Ceram. Soc.* 1992, **75**, 369–374.
27. Kobayashi, K., Yamaguchi, S., Tsunoda, T. and Imai, Y., Thermoelectric properties and defect structure of $La_{0.45}Nd_{0.45}Sr_{0.1}FeO_{3-\delta}$. *Solid State Ionics* 2001, **144**, 123–132.

28. Nakamura, T., Petzow, G. and Gauckler, L. J., Stability of the perovskite phase $LaBO_3$ (B = V, Cr, Mn, Fe, Co, Ni) in reducing atmosphere. I. Experimental results. *Mater. Res. Bull.* 1979, **14**, 649–659.
29. Katsura, T., Kitayama, K., Sugihara, T. and Kimizuka, N., Thermochemical properties of lanthanoid-iron-perovskite at high temperatures. *Bull. Chem. Soc. Jpn.* 1975, **48**, 1809–1811.
30. Peters, H. and Mann, G., Elektrochemische untersuchung des gleichgewichtes FeO + CO_2-reversible-FeO + CO. *Z. Elektrochem.* 1959, **63**, 244–248.
31. Huang, K., Tichy, R. S. and Goodenough, J. B., Superior perovskite oxide-ion conductor strontium- and magnesium-doped $LaGaO_3$: I, phase relationships and electrical properties. *J. Am. Ceram. Soc.* 1998, **81**, 2565–2575.